Thus, the propagation of elastic waves in a periodically laminated, saturated, porous medium has several important features which can be linked to the motion of the fluid relative to the skeleton at the boundaries between the layers. These features cannot be accounted for in the theory of visco-elastic media. They can be best accounted for within the framework of the Frenkel–Biot model.

LITERATURE CITED

1. Ya. I. Frenkel', "Toward a theory of seismic and seismo-electrical phenomena in moist soil," Izv. Akad. Nauk SSSR Ser. Georg. Geofiz., 8, No. 4 (1944).
2. M. A. Biot, "Theory of propagation of elastic waves in a fluid-saturated porous solid," J. Acoust. Soc. Am., 28, No. 2 (1956).
3. V. N. Nikolaevskii, K. S. Basniev, A. T. Gorbunov, et al., Mechanics of Saturation of Porous Media [in Russian], Nedra, Moscow (1970).
4. R. I. Nigmatulin, Principles of the Mechanics of Heterogeneous Media [in Russian], Nauka, Moscow (1978).
5. V. A. Barzam, "Calculation of the dynamic characteristics of seismic waves in saturated porous layered media," Izv. Akad. Nauk SSSR Fiz. Zemli, No. 10 (1984).
6. W. T. Thomson, "Transmission of elastic waves through a stratified solid material," J. Appl. Phys., 21, No. 2 (1950).
7. N. A. Haskell, "The dispersion of surface waves in multilayered media," Bull. Seismol. Soc. Am., 43, No. 1 (1953).
8. S. M. Rytov, "Elastic properties of a finely layered medium," Akust. Zh., 2, No. 1 (1956).
9. B. P. Sibiryakov, L. A. Maksimov, and M. A. Tatarnikov, Anisotropy and Dispersion of Elastic Waves in Laminated Periodic Structures [in Russian], Nauka, Novosibirsk (1980).
10. D. E. Uait, N. G. Mikhailov, and F. M. Lyakhovitskii, "Propagation of seismic waves in laminated media saturated with a liquid and gas," Izv. Akad. Nauk SSSR Fiz. Zemli, No. 10 (1975).
11. M. G. Markov and A. Yu. Yumatov, "Refraction of elastic waves at a crack located in saturated porous medium," Prikl. Mekh., 20, No. 8 (1984).

PROPAGATION OF COMPRESSION WAVES IN A POROUS FLUID-SATURATED MEDIUM

V. E. Dontsov, V. V. Kuznetsov, and V. E. Nakoryakov

UDC 532.546

Theoretical analysis of the propagation of compression waves in porous media saturated by a fluid [1-3] has shown that the main mechanism determining the evolution of the waves is interphase friction at the boundary of the fluid and the solid skeleton. It was found in [4-7] that one longitudinal wave is propagated in saturated porous media, while [6] presented test data on the decay of high-frequency acoustic waves which were generalized well by calculations performed in accordance with [1]. The authors of [8, 9], examining ultrasonic waves in consolidated porous media, were the first to experimentally detect the existence of two types of longitudinal waves – "fast" and "slow." The goal of the present study is to obtain experimental data on the dynamics of a compression wave in porous media saturated with fluid within a broad range of parameters of the waves and medium. We also want to generalize this data on the basis of calculations performed in accordance with well-known models.

Ignoring convective terms for the liquid and solid phases, the system of equations for the strains of the solid skeleton e_1 and the fluid e_2 in longitudinal waves has the following form in the unidimensional case [1, 10]

Novosibirsk. Translated from Zhurnal Prikladnoi Mekhaniki i Tekhnicheskoi Fiziki, No. 1, pp. 120-130, January-February, 1988. Original article submitted October 10, 1986.

0021-8944/88/2901-0111$12.50

$$\frac{\partial^2(\rho e_1 - \rho_2\xi)}{\partial t^2} - \frac{\partial^2(He_1 - C\xi)}{\partial x^2} = 0,$$
$$\frac{\partial^2(\rho_2 e_1 - \alpha\rho_2\xi/m)}{\partial t^2} - \frac{\partial^2(Ce_1 - M\xi)}{\partial x^2} - \frac{\partial T_V}{\partial x} = 0. \quad (1)$$

Here, T_V is the force of interphase friction per unit volume of the medium; $\frac{\partial T_V}{\partial x} = \frac{\nu\rho_2}{k_0}\frac{\partial \xi}{\partial t}$; $\xi = m(e_1 - e_2)$; $\rho = \rho_1(1 - m) + \rho_2 m$; ρ_1 and ρ_2 are the density of the solid and fluid phases; m is porosity; k_0 is permeability; ν is the kinematic viscosity of the fluid; α is the added mass of the fluid. The coefficients H, M, and C are functions of the bulk modulus K_B and shear modulus μ of elasticity of the porous skeleton, the bulk modulus of elasticity of the fluid K_2 and the material of the solid skeleton K_1, and porosity: $H = K_B + 4\mu/3 + (K_1 - K_B)^2/(D - K_B)$, $C = K_1(K_1 - K_B)/(D - K_B)$, $M = K_1^2/(D - K_B)$, $D = K_1(1 + m(K_1/K_2 - 1))$.

System (1) was obtained for low-frequency waves with the assumption that the process is quasi-steady, i.e., assuming that Darcy's law is valid in the flow of the fluid in the porous medium after the wave. For high-frequency compression waves, it is necessary to consider the process of establishment of the profile of fluid velocity in the porous medium. This leads to dependence of the force of phase interaction on the frequency of the process ω. In this case also, for harmonic waves, the dissipative term in (1) [1, 6, 10]

$$\partial T_V/\partial x = F(\omega)(\nu\rho_2/k_0)\partial\xi/\partial t, \quad (2)$$
$$F(\omega) = \frac{1}{4}\frac{sT(s)}{1 - 2T(s)/is}; \quad T(s) = \frac{\mathrm{ber}'(s) + i\,\mathrm{bei}'(s)}{\mathrm{ber}(s) + i\,\mathrm{bei}(s)},$$
$$s = (\omega/\omega_c)^{1/2}, \ \omega_c = m\nu/20k_0 \text{ for } s \ll 1, \ F(\omega) \approx 1.$$

The functions ber and bei are the real and imaginary parts of the Kelvin function, respectively.

Using the relationship between the strain of the solid skeleton and the fluid on the one hand, and the pressure in the fluid p and the first component of the tensor of effective stresses of the solid skeleton σ^f on the other hand [1, 2],

$$p = M\xi - Ce_1, \ \sigma^f = (H - C)e_1 - (C - M)\xi, \quad (3)$$

we transform system (1) as follows:

$$\frac{\partial^2\left[(\rho M - \rho_2 C)\sigma^f - (\rho(M - C) + \rho_2(H - C))p\right]}{\partial t^2} - (MH - C^2)\frac{\partial^2(\sigma^f - p)}{\partial x^2} = 0,$$
$$\frac{\partial^2\left[(\rho_2 M - \alpha\rho_2 C/m)\sigma^f - (\rho_2(M - C) + \alpha\rho_2(H - C)/m)p\right]}{\partial t^2} - (MH - C^2)\frac{\partial^2(-p)}{\partial x^2} - \frac{\nu\rho_2}{k_0}\frac{\partial\left[C\sigma^f + (H - C)p\right]}{\partial t} = 0. \quad (4)$$

System (4) is linear with respect to p and σ^f, and it can be solved by the method of rapid Fourier transformation [11] by expanding the initial signal into a discrete Fourier series and analyzing the propagation of each harmonic. To use this method, it is necessary to obtain the dependence of the wave number k on ω_n for system (4). Inserting $p = p_n\exp i(\omega_n t - kx)$ and $\sigma^f = \sigma_n\exp i(\omega_n t - kx)$ into (4) and considering the dependence of the dissipative processes on frequency (2), we obtain the dependence of k on ω_n

$$\left(\frac{k_{1,2}}{\omega_n}\right)^2 = \left[\left(\frac{\alpha\rho_2 H}{m} + \rho M - 2\rho_2 C - \frac{i\nu\rho_2 HF(\omega)}{k_0\omega_n}\right) \mp \right.$$
$$\mp\left[\left(\frac{\alpha\rho_2 H}{m} + \rho M - 2\rho_2 C - \frac{i\nu\rho_2 HF(\omega)}{k_0\omega_n}\right)^2 - \right.$$
$$\left.\left. - 4(MH - C^2)\left(\frac{\alpha\rho\rho_2}{m} - \rho_2^2 - \frac{i\nu\rho\rho_2 F(\omega)}{k_0\omega_n}\right)\right]^{1/2}\right][2(MH - C^2)]^{-1} \quad (5)$$

and the relationship between the amplitudes of the pressures $p_{n1,2}$ and the effective stress $\sigma_{n1,2}$ (the subscript 1 pertains to the first, "fast" wave, while the subscript 2 pertains to the second, "slow" wave)

$$\frac{p_{n1,2}}{\sigma_{n1,2}} = \left(\left(\frac{k_{1,2}}{\omega_n}\right)^2 - \frac{M\rho - C\rho_2}{MH - C^2}\right)\Big/\left(\left(\frac{k_{1,2}}{\omega_n}\right)^2 + \frac{C\rho - H\rho_2}{MH - C^2} - \frac{M\rho - C\rho_2}{MH - C^2}\right). \tag{6}$$

It follows from (5) that two types of waves having different velocities may propagate in one direction in a fluid-saturated porous medium. Here, a minus sign in (5) corresponds to a wave with the wave number k_1, while a plus sign corresponds to a wave with the wave number k_2. Figures 1a and b show characteristic relations for wave velocity c_Φ = Re(ω/k) and the attenuation factor η_Φ = Im(k(ω)).

Calculations were performed for parameters of the consolidated porous medium corresponding to the test conditions; lines 1 and 2 correspond to the velocity and attenuation of the first wave in a porous medium saturated with gasoline and oil, respectively, while lines 3 and 4 correspond to the second wave. It can be seen that the first wave propagates without dispersion or attentuation, while the second wave is strongly attenuated. For the first wave, the character of its evolution may be significantly affected by viscoelastic forces caused by the expulsion of fluid near points of contact of grains when they are deformed [10]. Allowance for these forces leads to dependence of the effective stresses on the strain rate $\sigma^f = (H - C)e_1 - (C - M)\xi + \beta\nu\rho_2\partial e_1/\partial t$, which for harmonic waves is equivalent to introduction of the operator H^* into Eq. (3) and system (1):

$$H^* = H + i\omega\beta\nu\rho_2. \tag{7}$$

Line 5 in Fig. 1b shows the results of calculation of attentuation of the first wave at $\beta = 4\cdot10^3$ with allowance for the occurrence of viscoelastic forces in the case of a porous medium saturated with oil.

With allowance for (5), the solution of system (4) has the form

$$p(x, t) = \sum_{n=0}^{L} p_{n,1}\exp i(\omega_n t - k_1(\omega_n)x) + \sum_{n=0}^{L} p_{n,2}\exp i(\omega_n t - k_2(\omega_n)x), \tag{8}$$

$$\sigma^f(x, t) = \sum_{n=0}^{L} \sigma_{n,1}\exp i(\omega_n t - k_1(\omega_n)x) + \sum_{n=0}^{L} \sigma_{n,2}\exp i(\omega_n t - k_2(\omega_n)x),$$

where $p_{n,1}$ and $\sigma_{n,1}$ pertain to the wave with k_1, and $p_{n,2}$ and $\sigma_{n,2}$ pertain to the wave with k_2. They are determined from the expansion of the initial signal into a discrete Fourier series

$$p(0, t) = \sum_{n=0}^{L}(p_{n,1} + p_{n,2})\exp(i\omega_n t),\ \sigma^f(0, t) = \sum_{n=0}^{L}(\sigma_{n,1} + \sigma_{n,2})\exp(i\omega_n t)$$

with the use of Eq. (6).

We will examine two types of boundary conditions in a fluid-saturated porous medium [3]: "fluid piston" – we assign the pressure in the fluid at the boundary with the porous medium $p(0, t) = \Delta p_0(t)$, and the effective stress $\sigma^f(0, t) = 0$; "impermeable piston" – we assign the first component of the stress tensor $\sigma(0, t) = \sigma^f(0, t) - p(0, t) = \Delta\sigma_0(t)$ and equate the strains of the solid skeleton and fluid $e_1 = e_2$.

With allowance for the above boundary conditions, we realized this method of solving system (4) on a computer. The results of the computations are shown below in comparison with experimental results.

The experiments were conducted on a unit of the "shock tube" type. On the first unit, the working section was a vertical thick-walled steel tube with an inside diameter of 10^{-2} m and a length of 0.54 m. This tube was filled with the porous medium. A fluoroplastic film $3\cdot10^{-5}$ m thick was located between the porous medium and the wall of the tube to prevent friction of the medium against the wall of the working section from affecting the propagation of the compression wave. The porous medium was a bed of sintered organic glass beads $(0.2\text{-}0.25)\cdot10^{-3}$ m in diameter. The beads were sintered directly in the working section. Before saturation with the fluid, the working section was evacuated with a force pump. This prevented the formation of air bubbles in the porous medium when it was filled with the fluid. In the experiments, we studied the propagation of two types of waves – stepped and bell-shaped. Profiles of stepped compression waves were obtained by the rupture of a diaphragm separating the high-pressure chamber from the working section. To realize the pre-

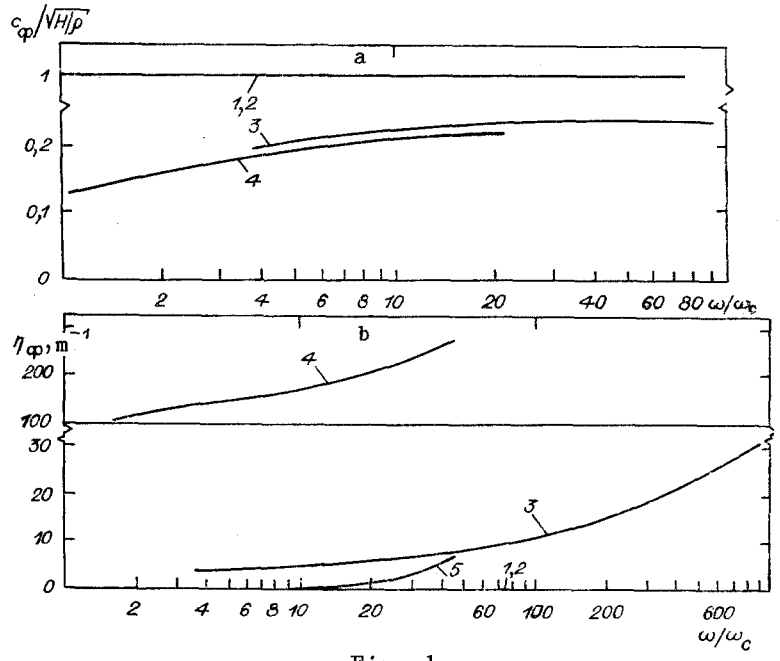

Fig. 1

scribed boundary conditions ("fluid" or "impermeable" pistons), bell-shaped pressure pulses were created by the impact of a piston against a thin layer of fluid on top of the porous medium or directly in the medium itself.

The second experimental unit had a working section in the form of a vertical thick-walled steel tube with an inside diameter of $53 \cdot 10^{-3}$ m. The tube was filled with a porous medium consisting of bulk bank sand with a particle diameter of $(0.1\text{-}0.5) \cdot 10^{-3}$ m. Clay and organic impurities were removed from the sand before it was used in the tests. The method of moist tamping was used to fill the working section with the medium. The sand was slowly poured into a container with fluid and carefully mixed to remove air bubbles. The fluid-saturated sand was then poured into the working section, tamped with a vibrating tool, and constricted by highly permeable porous plates. Given this method of medium preparation, porosity remains constant during the tests. The bell-shaped pressure pulses were created by the impact of a piston against the movable bottom of the fluid-filled transitional chamber. The piston was accelerated in an air shock wave. The pressure pulse formed in the transitional section propagated into the working section. The duration and amplitude of the initial pulse were varied by changing the weight of the piston and the pressure in the air shock wave. The resulting ranges of the parameters were as follows: intensity Δp_0 = 2-25 MPa; duration $\delta = (40\text{-}100) \cdot 10^{-6}$ sec (δ is the characteristic width of the signal at the level 0.37 Δp_0). The bulk modulus of elasticity of the skeleton K_B was increased by the constriction of the porous skeleton by the external load applied to the porous plate. To ensure a uniform load on the skeleton over its entire length, the working section was subjected to vibration during the constriction. The value of K_B was determined from the velocity of the compression wave in a dry bed with allowance for the relationship between the shear modulus of the solid skeleton μ and K_B [B]; $\mu = 1.1K_B$. The bulk modulus of the fluid was calculated from the velocity of a low-frequency compression wave measured in loose ($K_B \ll K_2$) sand saturated with fluid. Here, we used Wood's formula $v_B = ((m/K_2 + (1 - m)/K_1)\rho)^{-1/2}$.

Piezoelectric pressure gauges, with sensitive elements $2 \cdot 10^{-3}$ m in diameter, were placed along the working section. They did not touch the skeleton of the porous medium and measured the pressure profiles in the fluid phase. Signals from the gauges, sent through high-resistance amplifiers, were recorded on an oscillograph.

Figure 2 shows test data and calculated results (lines 1 and 2) on the evolution of the stepped pressure profile with an amplitude Δp_0 in a porous medium of organic glass beads saturated with gasoline and oil (a, b) at m = 0.35, $k_0 = 18 \cdot 10^{-12}$ m^2, $K_B = 1.2 \times 10^9$ N/m, $\mu = 0.41\ K_B$, $\alpha = 3.0$; oil – $\rho_2 = 0.86 \cdot 10^3$ kg/m^3, $\nu = 25.2 \cdot 10^{-6}$ m^2/sec, $K_2 = 1.51 \cdot 10^9$ N/m^2; gasoline – $\rho_2 = 0.75 \cdot 10^3$ kg/m^3, $\nu = 0.7 \cdot 10^{-6}$ m^2/sec, $K_2 = 0.86 \cdot 10^9$ N/m^2. It was found that two types of longitudinal waves – "fast" and "slow" – are propagated in a consolidated porous medium. It is not possible to distinguish between the waves at short distances into the medium (x = 0.015 m). However, the velocity of the "fast" wave v_1 is considerably greater

than that of the "slow" wave v_2, and at larger distances (x = 0.136 m) the waves can be separated (Fig. 2a). In the case of high fluid viscosities, dissipative processes greatly reduce the amplitude of the slow wave, and the latter cannot be detected after the waves separate. The fast wave, meanwhile, continues to propagate without attenuation (Fig. 2b). This leads to a marked change in the amplitude of the wave as a whole only in the region where the fast and slow waves separate. This region is located a short distance from the point of entry of the initial signal into the medium. The results of calculations at x = 0.015 and 0.136 m correspond to the overall pressure profile, while at x = 0 the results also give the initial pressure profile of the fast wave, with the amplitude Δp_{10}.

Figure 3 shows profiles of bell-shaped compression waves and compares these profiles with results calculated (lines 1 and 2) for different distances from the point of entry of a porous medium saturated with gasoline. Here, the parameters of the medium correspond to the values in Fig. 2a. The pressure profiles in Figs. 3a and b reflect the different methods of wave generation – "impermeable" and "fluid" pistons. The calculations show that with an impermeable piston, the slow wave nearly fails to form, while in the case of a fluid piston, the amplitude of the slow wave is comparable to the amplitude of the fast wave. The same result was obtained in the experiments. As for the stepped pressure profile, the amplitude of the fast wave in Fig. 3 undergoes almost no attenuation. This is due to the fact that the displacements of the solid skeleton and the fluid in the fast wave are close in value and are in phase, while their phases are opposite in the slow wave [1]. The best agreement between the test data and the calculated wave velocities for all of the experiments is seen at $\alpha = 3$. This value of α lies within the range $\alpha = 2$-3 obtained in [5] for highly constricted bulk glass beads; the quantity α has a significant effect on the velocity and rate of decay of the slow wave, but it has almost no effect on the parameters of the fast wave. It should be noted that in the calculations, the initial signal of bell-shaped form was approximated by the relation $\Delta p_0(t) = \Delta p_0 \exp(-(2t/\delta)^2)$ (δ is the characteristic length of the signal).

Figure 4 shows test data on the decay of the amplitudes of the fast (a) and slow (b) waves for different wave periods. Here, $\Delta p_{1,2}$ represents the amplitudes of the waves at a distance of 0.146 m from the point of entry to the medium, a: points 1 – porous medium, saturated with gasoline; 2 – kerosene; 3 – oil; b) 1, 2 – gasoline; 3, 4 – kerosene, with the wave amplitudes: 1, 3 – Δp_{20} = (0.1-0.3) MPa; 2, 4 – Δp_{20} = (0.6-0.8) MPa. For kerosene, $\rho_2 = 0.8 \cdot 10^3$ kg/m^3, $\nu = 1.7 \cdot 10^{-6}$ m^2/sec, $K_2 = 1.2 \cdot 10^9$ N/m^2.

In the investigated ranges of wave periods and medium parameters, the fast wave undergoes almost no attenuation. This finding is consistent with the calculated data (line 4).

The amplitude of the slow wave at the point of entry to the medium Δp_{20} was calculated from the measured amplitude of the fast wave in the same experiment by using the theoretical value for the ratio of the amplitudes of the fast and slow waves at the entry point. The calculated curves 5 for gasoline and 6 for kerosene satisfactorily generalize the test data for waves of an amplitude less than 0.3 MPa. At larger amplitudes, greater attenuation is seen for gasoline in the experiments than in the calculations. This is evidently due to an increase in interphase friction with an increase in Re. Thus, for amplitudes of (0.6-0.8) MPa, $\mathrm{Re} = \Delta u m d/\nu$ has a value of 30-40 in the second wave. With allowance for a binomial law, this gives an increase in interphase friction of 40% in the porous medium. The value of Re was determined from the relative velocity of the solid skeleton and the fluid in the wave Δu and the diameter of the beads d; Δu was evaluated from the relation $\Delta u = v_2 \xi / m$ by using Eq. (3) and calculated values of pressure and effective stress in the second wave.

It can be seen from Fig. 1 that the evolution of a fast wave at high frequencies can be significantly influenced by viscoelastic forces due to expulsion of fluid near points of contact of the solid particles during their deformation. Line 2 in Fig. 5 shows the character of evolution of the leading edge of a fast wave in an oil-saturated porous medium when the parameters of the medium correspond to Fig. 2b. Appreciable flattening of the leading edge of the wave is seen for short periods of time. Line 1 shows the calculation without allowance for viscoelastic forces, while line 3 shows the results obtained with the introduction of the complex modulus H^* by (7) with $\beta = 4 \cdot 10^3$. It is evident from a comparison of the experimental wave profile with the theoretical profile that viscoelastic effects have a greater influence on the evolution of a fast wave than does interphase friction. This should be considered in the calculations. It should be noted that the effect is quite small for the test data shown in Fig. 4a. Here, viscoelastic effects will be significant only in the cases of signals of considerably shorter duration or in the case of greater distances.

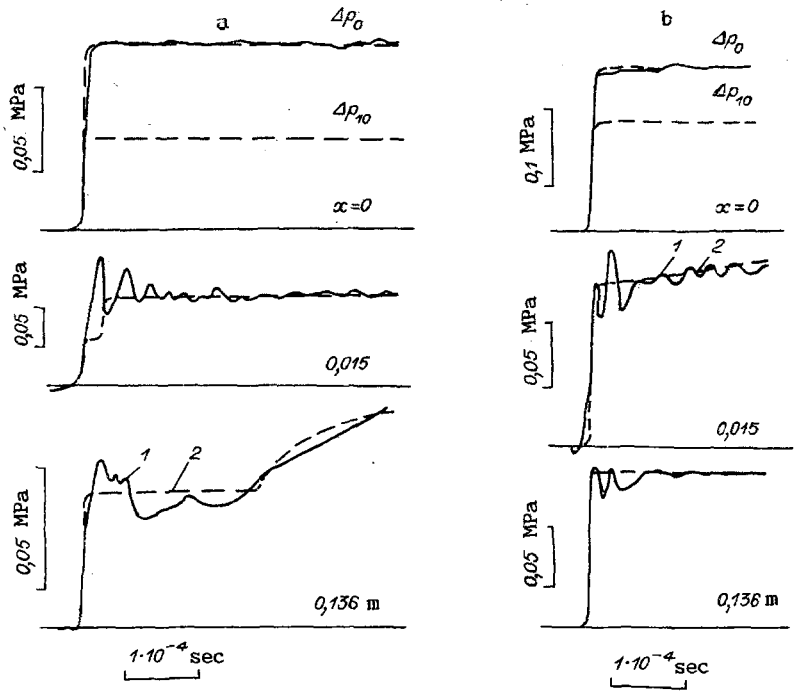

Fig. 2

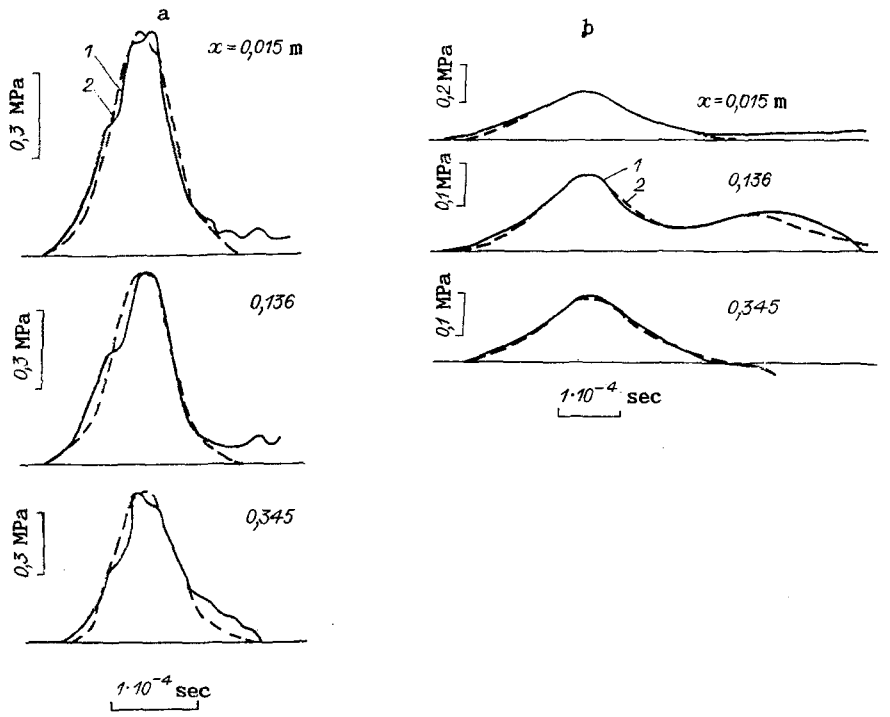

Fig. 3

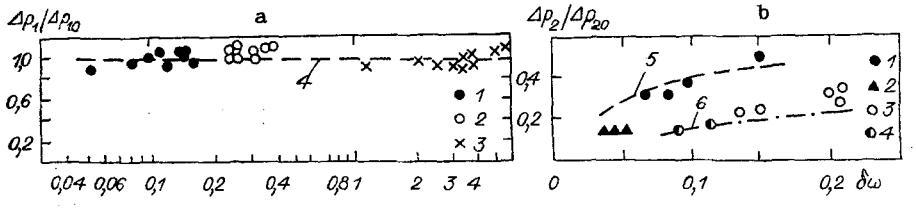

Fig. 4

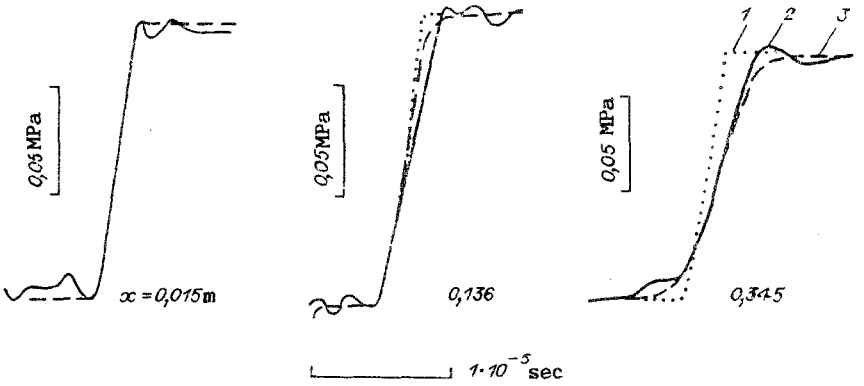

Fig. 5

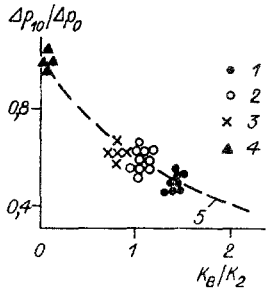

Fig. 6

The amplitudes of the fast and slow waves at the entry point are determined by the conditions of generation of the compression waves and the parameters of the medium. Figure 6 shows results of experiments with regard to the dependence of the amplitude of the fast waves at the entry point on the ratio K_B/K_2 with the "fluid" piston boundary condition: 1 corresponds to a porous medium saturated with gasoline, 2 corresponds to the same with kerosene, and 3 and 4 correspond to the same with oil. Also shown are results of calculations for all three types of fluids, which lie close to curve 5. The calculated results show that the amplitude of the fast wave, under the conditions of the experiments conducted here, depends only slightly on the viscosity and density of the fluid and is determined by the value of K_B/K_2 for the given skeleton material.

Figure 7 shows results on the dependence of the velocity of fast v_1 and slow v_2 waves on their amplitudes. Here, c_2 is the speed of sound in the fluid, $p_0 = 0.1$ MPa is the initial pressure in the medium; a: 1) test results for a porous medium saturated with gasoline; 2) kerosene; 3) oil; 4) calculation for gasoline; 5) kerosene; 6) oil; b: 1) test data for gasoline; 2) kerosene; 3) calculation for gasoline; 4) kerosene. In the investigated range of wave amplitudes, the velocities of the fast and slow waves are independent of their amplitudes. This confirms the correctness of using linear system (4) to analyze the process of wave propagation.

It was shown as a result of the completed tests that in bulk sand saturated with fluid, in the case where the bulk modulus elasticity of the skeleton is less than that of the fluid, a single longitudinal wave with the velocity v_1 is propagated. This velocity is close to the speed of sound in the fluid $c_2 = (K_2/\rho_2)^{1/2}$. Figures 8a and 9a show the character of evolution of bell-shaped compression waves over the length x of the working section. After the initial signal at x = 0, we took the profile of the compression wave in the porous medium 0.012 m from the point of entry. The fluid saturating the medium was oil with $\rho_2 = 0.86 \cdot 10^3$ kg/m^3, $K_2 = 1.25 \cdot 10^9$ N/m^2, $\nu = 32.4 \cdot 10^{-6}$ m^2/sec. The material of the solid skeleton had the parameters $\rho_1 = 2.56 \cdot 10^3$ kg/m^3, $K_1 = 40 \cdot 10^9$ N/m^2. The parameters of the porous skeleton in Fig. 8: $K_B = 0.1 \cdot 10^9$ N/m^2, m = 0.33, $k_0 = 24 \cdot 10^{-12}$ m^2; in Fig. 9: $K_B = 0.5 \cdot 10^9$ N/m^2, m = 0.3, $k_0 = 16 \cdot 10^{-12}$ m^2. It is evident that the amplitude of the compression wave decreases along x and that its period increases. The rate of decay of amplitude increases with an increase in K_B.

Figures 8b and 9b (line 1) show results of calculation of the evolution of the pressure perturbations. The parameters of the perturbations and the medium in the calculations correspond to the conditions of the tests. The initial bell-shaped signal was approximated

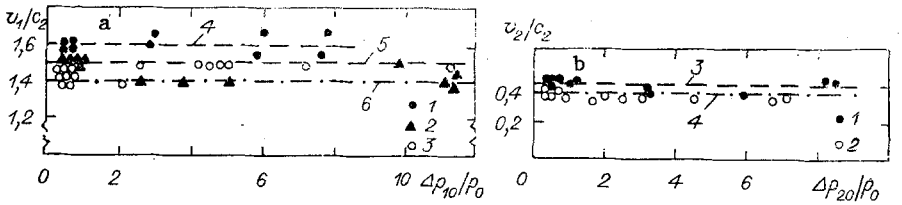

Fig. 7

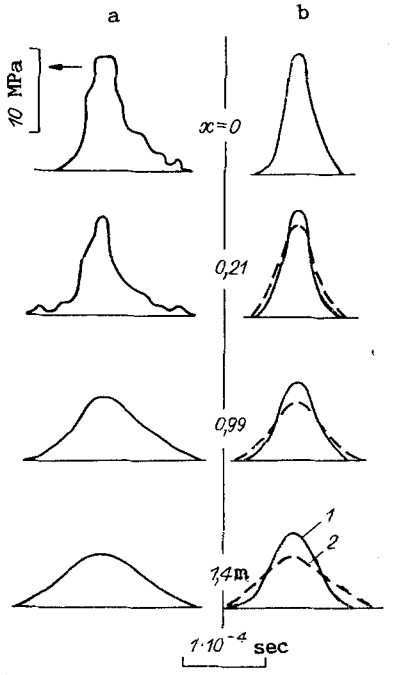

Fig. 8

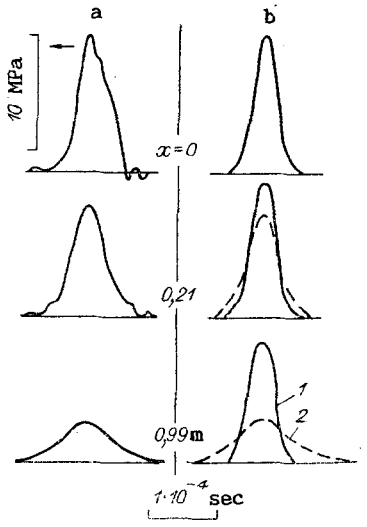

Fig. 9

in the calculations by the relation $\Delta p_0(t) = \Delta p_0 \exp(-(2t/\delta)^2)$. The added mass of the fluid was calculated from the formulas [6] $\alpha = 1 + (1 - m)/2m$.

The calculated results confirmed that, at $K_B < K_2$, only one longitudinal wave – a fast wave (using the terminology in [1]) – is propagated in the fluid-saturated porous medium. The second, slow wave decays very rapidly in the calculations and is not observed in experiments. Comparison of the calculated and experimental results in Figs. 8 and 9 showed that the fast wave decays more rapidly in the tests than in the calulations. Here, an increase in K_B in the tests leads to an increase in attenuation of the wave, while in the calculations it leads to a decrease in attenuation. This means that, in contrast to consolidated porous media, in bulk media an additional mechanism besides interphase friction is operative. In the propagation of compression waves in saturated porous media, particle displacements and friction losses between particles are possible. These events lead to the generation of forces associated with "dry" friction and, at low frequencies, such forces predominate over forces associated with interphase friction [12]. "Dry" friction can be allowed for in the case of harmonic waves by introducing the complex bulk modulus of elasticity $\bar{K}_B = K_B + iK_{BI}$ and complex shear modulus of elasticity $\bar{\mu} = \mu + i\mu_r$ of the solid skeleton [12] in place of the real values K_B and μ in linear system (4); K_{BI}/K_B and μ_I/μ increase slightly with an increase in skeleton strain e_1 and change within the range 0.03-0.07 for $10^{-5} < e_1 < 10^{-4}$ [13]. Comparison of the experimental results and the results calculated with the complex moduli $\bar{K}_B$ and $\bar{\mu}$ (line 2 in Figs. 8 and 9) showed that they agree well in regard to attenuation at $K_{BI}/K_B = 0.5$ and $\mu_I/\mu = 0.5$. For the test data in Figs. 8 and 9, $e_1 \sim 10^{-2}$. This is responsible for an increase in K_{BI}/K_B and μ_I/μ compared to the results [13] obtained for smaller e_1. The strains were evaluated from (3) $e_1 \approx \Delta p_0 m/K_2$.

With a wave velocity measurement error of 5%, the measured values of wave velocity v_1 = 1360 and 1590 m/sec (Figs. 8 and 9) agree with the calculated values. It should be noted that the introduction of the complex moduli has almost no effect on wave velocity. Comparison of the test results and calculations for $\alpha = 1$ on the one hand, and the results calculated from the expression in [6] on the other hand, showed that α has no effect on the propagation and rate of decay of a fast wave.

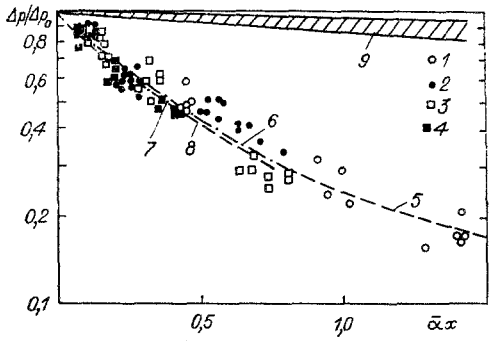

Fig. 10

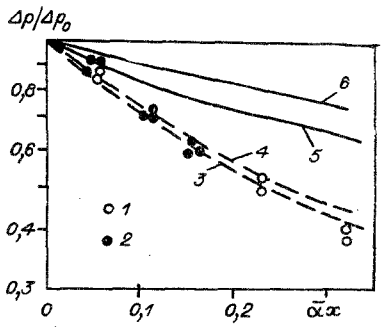

Fig. 11

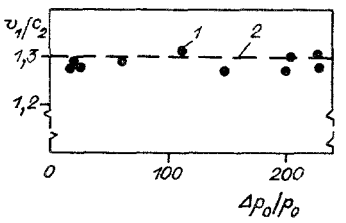

Fig. 12

Analysis of the experimental data in Figs. 8 and 9 showed that the attenuation of compression waves in a bulk porous medium is determined mainly by the presence of "dry" friction. For low frequencies $\omega < \omega_c = m\nu/20k_0$ and at $K_B < K_2 \ll K_1$, if we replace the real values of the moduli K_B and μ by their complex analogs $\bar{K}_B = K_B + iK_{BI}$ and $\bar{\mu} = \mu + i\mu_I$ and consider "dry" friction between particles of the porous medium, then from (5) we obtain an expression for the velocity and attenuation factor of harmonic waves $v_1 = (H/\rho)^{1/2}$, $k_I = \ln(\Delta p/\Delta p_0)/x = \alpha_\nu + \alpha_I$, where Δp is the amplitude of the wave at the distance x from the point of entry to the medium. The coefficient $\alpha_\nu = k_0\omega^2(\rho - \rho_2)^2/(2\nu v_1\rho\rho_2)$ describes dissipative losses to interphase friction, while $\alpha_I = (K_{BI} + 4\mu_I/3)\omega/(2v_1(K_2/m + K_B + 4\mu/3))$ accounts for "dry" friction between particles of the porous medium.

For low frequencies $\omega \ll \frac{\rho\rho_2\nu(K_{BI}+4\mu_I/3)}{k_0(\rho-\rho_2)^2(K_2/m+K_B+4\mu/3)}$, we can ignore dissipation at the phase boundary and $k_I = \alpha_I \sim \omega$. The linearity of the attenuation factor with respect to frequency can be used to generalize data on the attenuation of pressure pulses by changing over from the characteristic pulse width δ to its characteristic frequency $\omega_* = 1/\delta$.

Figure 10 shows experimental results on the attenuation of bell-shaped compression waves in bulk sand saturated with fluid with $K_B = 0.5\cdot10^9$ N/m^2, $m = 0.3$, $k_0 = 16\cdot10^{-12}$ m^2 for different δ, Δp_0, and ν. Here, $\alpha = (K_{BI} + 4\mu_I/3)/(2v_1\delta(K_2/m + K_B + 4\mu/3))$. Curves 1 and 2 were obtained for sand saturated with kerosene with $\rho_2 = 0.79\cdot10^3$ kg/m^3, $\nu = 1.54\cdot10^{-6}$ m^2/sec, $K_2 = 0.9\cdot10^9$ N/m^2, while curves 3, 4 were obtained for oil with $\rho_2 = 0.86\cdot10^3$ kg/m^3, $\nu = 32.4\cdot10^{-6}$ m^2/sec, $K_2 = 1.25\cdot10^9$ N/m^2; for curves 1 and 3, $\delta = (45\text{-}55)\cdot10^{-6}$ sec, $\Delta p_0 =$ 7-25 MPa, while for curves 2 and 3, $\delta = (80\text{-}100)\cdot10^{-6}$ sec, $\Delta p_0 =$ 2-5 MPa.

The results of calculatons of wave amplitudes at different distances x from the point of entry to the porous medium are shown by lines 5-8 in Fig. 10. The results correspond to the test conditions and allow for both dry friction ($K_{BI} = 0.5\ K_B$, $\mu_I = 0.5\ \mu$) and dissipation at the phase boundary. Lines 5 and 6 show results for a porous medium saturated with kerosene, and 7 and 8 show results in the case of oil as the fluid. Here, $\delta = 48\cdot10^{-6}$ sec for 5 and 7 and 10^{-4} for 6 and 8. the test data is satisfactorily generalized by the theoretical relations. In the dimensionless coordinates used here, the two sets of results nearly coincide for different parameters of the perturbations and medium. The agreement between the results can be attributed to the slight effect of dissipation at the phase boundary on decay of the wave amplitude. Calculated results, without allowance for dry friction $K_{BI} = \mu_I = 0$ for the same parameters lie within region 9 and show considerably less attenuation than the experiments. The deviation of the theoretical relations 5-8 from the straight lines in the given coordinates is connected with an increase in wavelength over the length of the working section (Figs. 8 and 9), which leads to a decrease in ω_* and in the rate of wave decay during evolution. We took constant values for the imaginary moduli in

the calculations throughout the investigated range of wave amplitudes Δp_0 = 2-25 MPa: $K_{BI} = 0.5\ K_B$, $\mu_I = 0.5\ \mu$. In reality, K_{BI}/K_B and μ_I/μ increase slightly with an increase in the wave amplitude due to an increase in skeleton strain e_1 [13]. Allowance for $K_{BI}(\Delta p_0)$ and $\mu_I(\Delta p_0)$ leads to convergence of the test data for waves of large 1, 3 and small 2, 4 amplitude and theoretical relations 5-8.

Figure 11 shows test results on the attenuation of compression waves in a porous bulk medium with $K_B = 0.1 \cdot 10^9$ N/m^2 for $\delta \approx 48 \cdot 10^{-6}$ and 10^{-4} sec (points 1 and 2) at m = 0.33, $k_0 = 24 \cdot 10^{-12}$ m^2, and $\nu = 32.4 \cdot 10^{-6}$ sec. The medium is saturated with oil. Lines 3 and 4 show calculated results with allowance for dry friction, while 5 and 6 show the same without allowance for dry friction. Calculated curves 3 and 5 correspond to $\delta = 48 \cdot 10^{-6}$ sec, while 4 and 6 correspond to $\delta = 10^{-4}$ sec. The role of dissipative processes at the phase boundary increases with a decrease in K_B, which leads to greater divergence of curves 3 and 4 in the dimensionless coordinates considering only the role of dry friction in Fig. 11.

Figure 12 compares experimental and theoretical results on the dependence of wave velocity on the initial intensity in sand saturated with oil with $K_B = 0.5 \cdot 10^9$ N/m^2. The parameters of the medium correspond to the parameters in Fig. 10. Here, p_0 is the initial pressure in the fluid, 1 shows experimental results, and 2 shows results calculated with $K_{BI}/K_B = 0.5$ and $\mu_I/\mu = 0.5$. The test data on velocity are independent of the amplitude of the initial signal and agree well with the theoretical value.

Thus, we have confirmed the correctness of using the linear equations in [1-3] and the method of calculation to describe the evolution of a signal in the range of wave amplitudes investigated above.

We thank Z. M. Orenbakh for writing the program for numerical realization of the method of rapid Fourier transformation.

LITERATURE CITED

1. M. A. Biot, "Theory of propagation of elastic waves in a fluid-saturated porous solid," J. Acoust. Soc. Am., 28, No. 2 (1956).
2. R. I. Nigmatulin, Principles of the Mechanics of Heterogeneous Media [in Russian], Nauka, Moscow (1978).
3. V. E. Nikolaevskii, K. S. Basniev, A. T. Gorbunov, and G. A. Zotov, Mechanics of Saturated Porous Media [in Russian], Nedra, Moscow (1970).
4. G. M. Lyakhov, Principles of the Dynamics of Blast Waves in Soils and Rocks [in Russian], Nedra, Moscow (1974).
5. S. N. Domeniko, "Elastic properties of unconsolidated porous sand reservoirs," Geophysics, 42, No. 7 (1977).
6. D. Salin and W. Schon, "Acoustics of water-saturated packed glass spheres," J. Phys. Lett., 42 (1981).
7. J. M. Hovem and J. D. Ingram, "Viscous attenuation of sound in saturated sand," J. Acoust. Soc. Am., 66, No. 6, (1979).
8. T. J. Plona, "Observation of a second bulk compressional wave in a porous medium at ultrasonic frequencies,: Appl. Phys. Lett., 36, No. 4, (1980).
9. D. L. Johnson and T. J. Plona, "Acoustic slow waves and the consolidation transition," J. Acoust. Soc. Am., 72, No. 2 (1982).
10. R. D. Stoll, "Theoretical aspects of sound transmission in sediments," J. Acoust. Soc. Am., 68, No. 5 (1980).
11. Z. M. Orenbakh, Interphase Heat Transfer and the Dynamics of Pressure Perturbations in Boiling Liquids: Physical-Mathematical Sciences Candidate Dissertation, ITF SO AN SSSR, Novosibirsk (1984).
12. R. D. Stoll, "Acoustic waves in water-saturated deposits," in: Acoustics of Marine Deposits [Russian translation], Mir, Moscow (1977).
13. J. B. Hall and F. E. Richart, "Dissipation of elastic wave energy in granular solid," J. Soil Mech. Found Div. A. S. C. E., 89, No. SM6 (1963).